J Mater Sci (2007) 42:6469–6476
DOI 10.1007/s10853-006-1250-x

The physical and photo electrochemical characterization of the crednerite $CuMnO_2$

Yassine Bessekhouad · Yamina Gabes · Aissa Bouguelia · Mohamed Trari

Received: 30 May 2006 / Accepted: 10 November 2006 / Published online: 25 April 2007

Abstract $CuMnO_2$ is prepared via $Cu^+ \rightarrow Li^+$ exchange in molten copper (I) chloride. It crystallizes in a monoclinic structure (SG *C2/m*) where the MnO_6 octahedra elongation is ascribed to the Yahn–Teller (Y–T) effect of Mn^{3+} ions. From chemical analysis, the oxide is more accurately formulated as $CuMnO_{2.01}$. Above 250 °C, it undergoes a reversible transition to spinel $Cu_xMn_{3-x}O_4$ and beyond 940 °C it converts back to $Cu_{1.1}Mn_{0.9}O_2$. Extrapolation of high-temperature magnetic data indicates *T*-intercept θ_p of –450 K and an effective moment of 5.22 μ_B, consistent with strong antiferromagnetism in the basal plans and high spin (HS) configuration Mn^{3+}. This value is slightly larger than that of the spin only moment, a behavior ascribed to Cu^{2+} originating from oxygen insertion. As prepared, $CuMnO_2$ displays p-type conductivity with an activation energy of 0.16 eV. Most holes generated upon band gap excitation are trapped on Cu^+ ions and the conduction occurs by small polarons hopping between neighboring sites. The linear increase of thermopower for $Cu_{1.05}Mn_{0.95}O_2$ with temperature indicates a hole mobility $\mu_{300\ K}$ (3.5×10^{-6} cm^2 V^{-1} s^{-1}) thermally activated. $CuMnO_2$ is made p- and n-type and the difference in the carriers mobilities is attributed to different oxygen polyhedra. The title oxide, characterized photo electrochemically, exhibits a pH-insensitive flat band potential (+0.13 V_{SCE}). The valence band, located at 5.3 eV below vacuum, is made up of Cu 3d orbital. As application, the powder showed a good performance for the H_2-photo evolution.

Y. Bessekhouad · Y. Gabes · A. Bouguelia · M. Trari (✉)
Laboratoire de Stockage et de Valorisation des Energies Renouvelables, USTHB, BP 32 El-Alia, 16111 Algiers, Algeria
e-mail: mtrari@caramail.com

Introduction

The renewable energies utilization continues to attract much attention [1, 2] and we emphasize the importance of seeking new materials for the solar energy transformation. To overcome drawbacks caused by wide forbidden band (E_g) and low lying valence band (VB) of O^{2-}:2p parentage typical of most oxides, owing to its high electron affinity, investigations were oriented towards materials with new crystalline structure. Our interest focused on $A^+B^{3+}O_2$ family deriving from the delafossite structure typified by the mineral $CuFeO_2$, A is commonly a monovalent metal and B any one of 3d transition metals [3]. This class of materials exists with moderate gap E_g that confers them an efficient use of the sun spectrum. The E_g-values are around 1.4 eV, close to the optimal value required for terrestrial applications. On the other hand, the transport properties are governed by the A-atom and vary from near metals (A = Pd or Pt) [4] to insulators (A = Cu or Ag) [5]. However, because of their layered structure, oxygen can be reversibly intercalated and $CuBO_2$ are available as p-type semiconductors (SC). The electric properties were slightly improved by doping process [6], the increase of the conductivity with the temperature indicates that the charge carriers are likely polaronic with enhanced carrier mobility. The open literature of recent years has referred to some physical properties of $CuBO_2$ and one of practical applications is the light to chemical energy conversion. This fact was confirmed recently in our laboratory by their use as H_2-electrode under visible light [7, 8]. However whereas little is known about its physical properties, the photo electrochemical (PEC) studies have never been investigated. It is now well established that the electrical and magnetic properties of $CuBO_2$ strongly depend on the preparative conditions and particularly on the structure

type of the precursor [9]. The aim of the present work is to improve the knowledge toward the transport and magnetic properties of the crednerite $CuMnO_2$ prepared by exchange reaction with $LiMnO_2$ in molten copper(I) chloride (melting point 480 °C) under O_2-free atmosphere. $CuMnO_2$ is classified as a narrow band SC and the PEC properties are reported for the first time. The exchange method yields a high specific surface area with enhanced photocatalytic properties.

Experimental

$CuMnO_2$ was synthesized by exchange reaction: $CuCl + LiMnO_2 \rightarrow CuMnO_2 + LiCl$ the starting products were homogenized in a dry box and sealed in a Pyrex ampoule under low pressure. The mixture was heated at 520 °C for 5 days and $CuMnO_2$ was recovered as brown powder by leaching out with deionized water. The precursor $LiMnO_2$ was prepared from Mn_2O_3 and dried Li_2CO_3 with a 5% weight excess. The powdered reagents were intimately mixed and fired in an alumina boat under pure Ar flow at 880 °C with an isothermal plateau at 650 °C for 6 h. This operation precludes the loss of Li_2O by volatilization resulting in the apparition of spinel $LiMn_2O_4$ lines in the X-ray diffractometry (XRD) pattern. Generally two grindings and firings were required to achieve well-crystallized oxides. The commercial grade Ar was deoxygenated by flowing the gas over a bed of iron fillings at 500 °C. For PEC characterization, $CuMnO_2$, n-$CuMn_{0.97}Sn_{0.03}O_2$, p-$CuMn_{0.97}Ca_{0.03}O_2$ and p-$Cu_{1.05}Mn_{0.95}O_2$ were elaborated by solid state reaction as reported previously [10] except that the starting oxides were CuO, Cu_2O, SnO_2, CaO, MnO and Mn_2O_3 all of purity >99.99%. The prefired binary oxides, in stoichiometric amounts, were homogenized in an agate mortar, cold pressed into pellets and sealed in silica tubes under dynamic vacuum (~2 mbar). The tubes were then fired at 960 °C for 48 h with intermediate regrindings, the pellets have good mechanical properties and the compactness lies between 70% and 75%. Mn_2O_3 was obtained by firing pure MnO_2 at 850 °C overnight and air quenched whereas CaO was prepared from $CaCO_3$ decomposition at 700 °C just prior use.

The end products were characterized by XRD using Cu Kα radiation. The diffraction data were recorded for 40 s at each 0.02° step over a 2θ range from 5° to 80°. The lattice constants were determined from corrected peak positions using Si as standard and a least square refinement program. The density of $CuMnO_2$ was obtained from the hydrostatic weighting in toluene by using an electronic balance (sensitivity of 10^{-4} g); the sample was heated to eliminate adsorbed water. The elemental analysis (Cu and Mn contents) of $CuMnO_2$ was carried out by inductively coupled plasma emission (Varian Vista-Pro-CCD, Simultaneous ICP-OES). Iodometric titration has been used to determine the nominal oxidation state of copper. Approximately 40 mg of oxide was dissolved in HCl with KI excess under inert atmosphere, the liberated iodine was back titrated by $Na_2S_2O_3$ (0.1 M). The thermal analyses (TGA/DTG) were performed in air with a heating rate of 3 °C min^{-1} using a computer-controller thermo balance Setaram (Setsys 16/18).

The magnetic susceptibility $\chi_M(T)$ was measured in the range 4.2–460 K in the heating direction with a Faraday balance under a magnetic field of 20,000 G, $\chi(T)$ was corrected by subtracting the orbital diamagnetism from cores of relevant ions [11]. The EPR spectrum was recorded in a Bruckner 115 spectrometer. The electrical resistivity ρ was measured by the dc four-probe method using a current of 1 mA and the thermopower data α ($=\Delta V/\Delta T$) were obtained thanks to an equipment described elsewhere [12].

Electrical contact with copper wires was made on the backside of pellets with silver paint. The pellets were then embedded in glass holders with resin epoxy leaving an exposed area of 0.19 cm^2. The standard PEC set up, used for the intensity–potential $J(V)$ characteristics, was composed by a Pyrex electrochemical cell, a potentiostat Voltalab 201 and a 200 W tungsten lamp as a light source equipped with a concentrator and a reflector (74 mW cm^{-2}). A Pt-counter electrode (1 cm^2) was employed as auxiliary electrode and all the potentials were quoted against a saturated calomel electrode (SCE). The oxygen-free KOH solution (suprapure), used to maintain high electro conductivity, was continually deoxygenated by nitrogen. The point of zero zeta potential (pzzp) has been accurately determined by measuring the equilibrium pH of an aqueous solution containing a suspension of powdered oxide. The procedure and apparatus for the H_2-photogeneration have been described elsewhere [13]. The solutions were prepared from analytical reagents and doubly distilled water.

Results and discussion

The low-temperature preparation via exchange reactions in molten baths is a useful technique for the formation of some oxometallates that cannot be obtained by ceramic route. The synthesis was carried out in sealed ampoules to preclude oxidation of manganese. The analysis of $CuMnO_2$ by ICP indicated a Cu/Mn equal to unity within the experimental errors. Cu^+ is less oxidant than Mn^{3+} and in the crystal lattice; the formulation (Cu^+/Mn^{3+}) was counterbalanced by the reticular energy. In acidic media, the equilibrium $CuMnO_{2+\delta(solid)} \leftrightarrow Cu^{2+}{}_{aq.} + Mn^{2+}_{aq.}$ lies strongly to the right hand side. This allowed the

determination of copper oxidation state by iodometry, an average valence of 1.03 was found which would correspond formally to a δ-value of 0.015. The XRD spectrum of $CuMnO_2$ (Fig. 1), virtually free from impurities, was successfully indexed in a monoclinic symmetry; all the peaks are assigned to the crednerite phase (SG *C2/m*, No. 12). The measured density (5.305) agrees with that calculated on the basis of two formula weights by unit cell (5.418). Figure 2 shows an assemblage of TGA/DTG plots performed in air, TGA reveals an oxygen gain at ~250 °C and peaks at 620 °C accounting for 5.39% of the total initial mass and which results in the reversible transition into oxygen rich spinel $Cu_xMn_{3-x}O_4$ (x = 1.03) according to the reaction:

$$CuMnO_2 + \frac{1}{2(3-x)}O_2 \rightarrow \frac{1}{3-x}\,Cu_xMn_{3-x}O_4 + \frac{3-2x}{3-x}CuO$$

Further firing (>940 °C) shows an oxygen loss of 1.11% which converts back the oxide to the crednerite $Cu_{1.1}Mn_{0.9}O_2$ and where the residual spinel exists as impurity. DTG exhibits a first peak at 434 °C and a second one at 952 °C indicating that the respective formation of the spinel and the crednerite occur in one-step reaction. At 1,150 °C, $CuMnO_2$ melts peritectically and XRD analysis indicated the coexistence of cubic spinel phase and CuO/Cu_2O, a result confirmed by the absence of peaks in the DTG plot during back scanning when the sample was slowly cooled. The composition $Cu_{1.1}Mn_{0.9}O_2$ has been determined by interpolation from a constructed calibration plot of lattice constants a and c as a function of composition x in $Cu_{1+x}Mn_{1-x}O_2$ [14]. Both a and c increase approximately linearly with composition ($0 \leq x \leq 0.20$) following the Vegard's law and this means that $Cu_{1+x}Mn_{1-x}O_2$ is a substitutional system throughout the whole composition

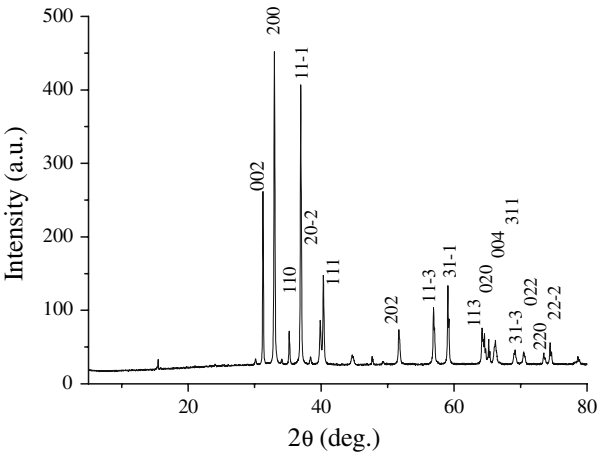

Fig. 1 Powder XRD pattern of $CuMnO_2$ prepared by exchange reaction

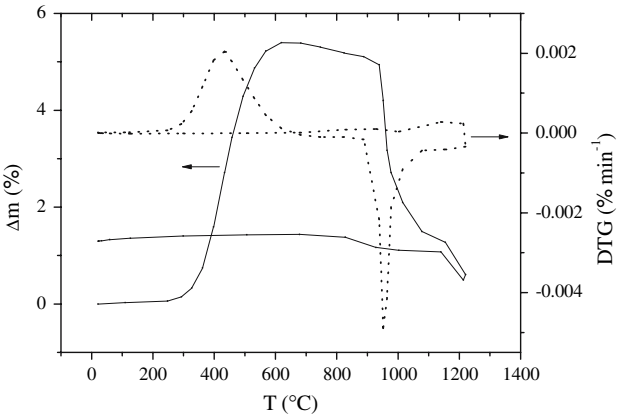

Fig. 2 Combined TG/DTG of $CuMnO_2$ in air, heating rate 3 °C min^{-1}

range. Given that the lattice constants do not change for $x > 0.20$, the latter value can be considered as the upper boundary of the solid solution. The parameters for other delafossites are gathered in Table 1 along with the selected physical properties.

Unique among $CuBO_2$ congeners, the structure of $CuMnO_2$ closely resembles that of delafossite. It consists of a close-packed oxygen sheets in which the octahedral sites are occupied by Mn^{3+} ions. The MnO_6 octahedra share six edges to form infinite $\{MnO_2^-\}_\infty$ layers connected to each other by Cu^+ linearly bonded to two oxygen to form $(O–Cu–O)^{3-}$ ''dumb-bell'' parallel to c-axis. Each Cu^+ is surrounded by six coppers hexagonally arranged in the (a, b) plan. One of authors noted the anisotropy whose structure was later established on single crystal [15]. The unusually large c/a value results from strong elongation of MnO_6 octahedra, ascribed to the Y–T ion Mn^{3+}. The effect of the distortion of Y–T ions on the mean bond lengths has been reported early, the Mn–O distances do not agree with those predicted when the effective ionic radii are used [16]. There are four in plans Mn–O bonds at 0.1929 nm and two apical Mn–O at 0.2260 nm [15] leading to an axial elongation $Mn–O_{\parallel}/Mn–O_{\perp}$ of 1.17. The octahedron coupling leads to zigzag shaped rows along the [010] direction doubling thus the b-parameter. The symmetry is lowered from hexagonal to monoclinic implying a lift of degeneracy of Mn^{3+} 3d orbital with an electronic configuration t_{2g}^3 $d_{x^2-y^2}^2 - d_{z^2}^1$. This ion exchangeable structure allowed us to prepare a new phase $AgMnO_2$ in silver nitrate non-cited in the literature. The reaction occurred in aqueous solution ($CuMnO_2 + AgNO_3 \rightarrow AgMnO_2 + Cu^{2+} + 2NO_3^-$), over time the solution turned to blue an evidence of the formation of $Cu(H_2O)_6^{2+}$ complex [17]. The IR spectra gives valuable informations on the M–O stretching, the sites of ions can be identified in the light of our data and that reported in the literature [18]. The absorption bands in the range 200–1,000 cm^{-1} are generally assigned to optically

Table 1 Cell parameters of $CuMnO_2$ based oxides

Compound	*a* (nm)	*b* (nm)	*c* (nm)	*β* (°)
$CuMnO_2$-D	0.5596(2)	0.2880(1)	0.5899(2)	104.02
$CuMnO_2$-E	0.5596(2)	0.2884(6)	0.5890(0)	103.94
$Cu_{1.05}Mn_{0.95}O_2$	0.5572(4)	0.2886(6)	0.5894(8)	104.32
$CuMn_{0.97}Ca_{0.03}O_2$	0.5603(6)	0.2883(7)	0.5894(6)	104.00
$CuMn_{0.97}Sn_{0.03}O_2$	0.5598(3)	0.2885(1)	0.5895(4)	104.07

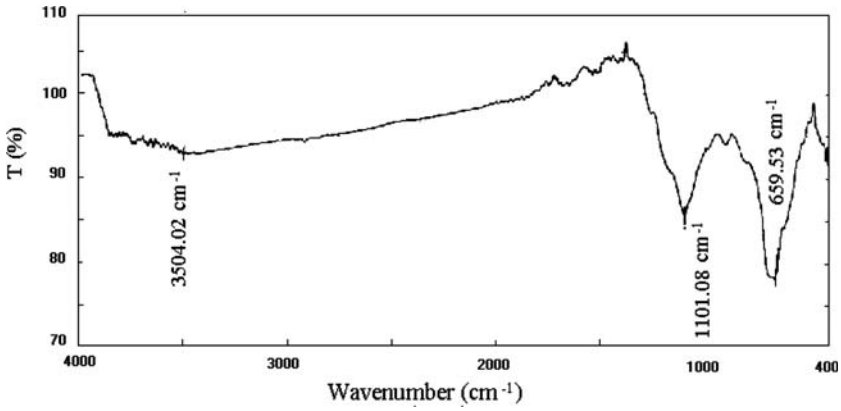

Fig. 3 IR spectra of $CuMnO_2$ at room temperature

active vibrations of ions in inorganic oxides. There is one vibrational stretching located at 1,101 cm^{-1} and associated with Mn^{3+} in octahedral sites whereas the peak centered at 659.5 cm^{-1} is ascribed to linear entities CuO_2^{3-} (Fig. 3).

As mentioned in introduction, the magnetic properties of delafossites are sensitive to preparative conditions. The thermal variation of the reciprocal susceptibility χ_M^{-1} of $CuMnO_2$ (Fig. 4) exhibits a sharp minimum at $T_C \sim 140$ K, characteristic of a low dimensionality, suggesting an onset of antiferromagnetism order. At high temperature, $\chi_M^{-1}(T)$ obeys a Curie–Weiss law $\chi_M^{-1} = (T - \theta_p)/C$ and the extracted constants obtained by the least square fitting, in a temperature range extending over ~150 K, are $\theta_p = -450$ K and $C = 3.41 \pm 0.02$. It is quite interesting to note that the experimental effective moment (5.22 μ_B) is slightly larger than that expected for ^5D state of HS Mn^{3+} $\{S = (2s(s + 1))^{0.5}, \mu_B = 4.91\ \mu_B\}$. This fact is attributed to oxygen insertion, which generates divalent copper with one unpaired electron ($3d^9$, $S = 0.5$) contributing to the increase of paramagnetism. At 4.2 K, the variation of χ_M was found to be field dependent and increases in the range 0–18,000 G [19], a behavior which could be attributed to the anisotropic effect given by ($\chi_M = \chi_\perp + \chi_{||}$) for polycrystalline oxide, $\chi_\perp$ and $\chi_{||}$ are respectively the perpendicular and parallel susceptibility contributions. χ is found to increase more rapidly at 4.2 K indicating that $\chi_\perp$ is larger than$\chi_{||}$. No ferromagnetic component was observed at 4.2 K excluding a canted antiferomagnetism.

The EPR spectra of $CuMnO_2$ (Fig. 5) shows a single broad signal ($\Delta H_{pp} \sim 1{,}000$ G) with a *g*-value of 2.008. The broadening of the peak can result from the axial elongation of the MnO_6 octahedra and is correlated to the degree of the distortion of the Mn^{3+} site based on structural data. An investigation of the line width requires an accurate determination of the zero field splitting which contributes largely to broadening to the line which should diverge when one approaches the Neel temperature from above. The large θ_p-values suggest strong antiferromagnetic interactions in the plans (001) and $CuMnO_2$ is a promising candidate for a two dimensional antiferromagnetic lattice. Indeed, each Mn layer is intercalated by three non-magnetic sheets and one can expect a good realization of a 2D model where Mn–Mn intraplane interactions would be dominated. The coupling occurs between half filled d_{z^2} orbitals and the exchange integral *J* was estimated from the T_C-simply as usually done [20]:

$$\frac{J}{k} = \frac{3T_C}{2zS(S+1)}$$

where *z* is the number of nearest neighbors (=6). The calculated value (–5.9 K) is about two fold lower than that found previously (–14 K) [10].

The large anisotropy is common in $CuBO_2$ and the pellets consist of randomly oriented microcrystals. The inter Cu length (0.2884 nm = *b* parameter) is greater than the expected one for 3d electrons collective behavior like in

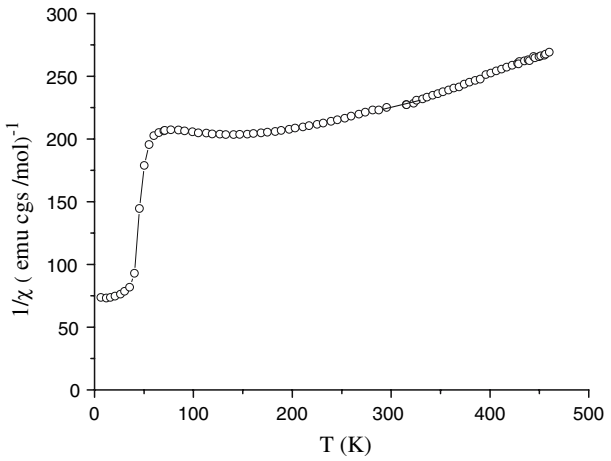

Fig. 4 The thermal variation of the reciprocal magnetic susceptibility of $CuMnO_2$

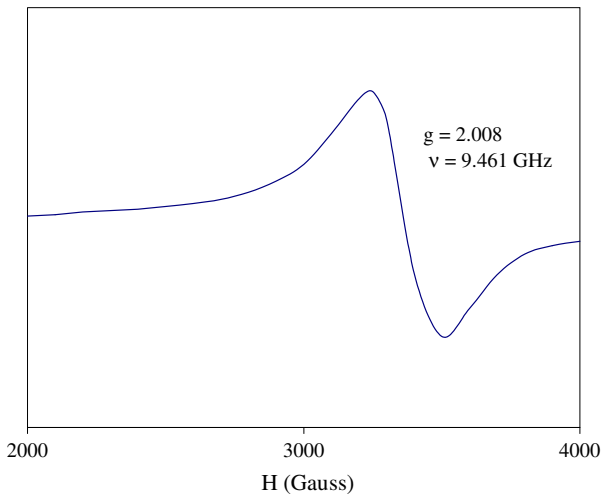

Fig. 5 EPR spectra of $CuMnO_2$ at room temperature

metal copper (0.2550 nm)[1] [21] and $CuMnO_2$ is predicted to be a SC ($d\rho/dT < 0$) according to the earlier energy diagram of CuO_2^{3-} [22]. Figure 6 shows that $\log(1/\rho)$ is proportional to $\exp(\Delta E_\rho/kT)$, the data were fitted by a least square method to a straight line and the activation energy ΔE_ρ was calculated from the slopes. $CuMnO_2$ can be made n- and p-type and the large ΔE-values (Table 2) are in conformity with a conduction mechanism by small polarons hopping. The electron mobility λ_e ($=eN_A\rho$) in n-type specimen is lower by two order of magnitude than that of holes in p-type one. This can be inferred to the electrons hopping between $Mn^{2+/3+}$ through edge-shared octahedra obstructed by oxygen coordination. The electrons must overcome a further potential barrier unlike to hole hopping

[1] Copper crystallizes in a body centered cubic with a lattice constant of 0.256 nm.

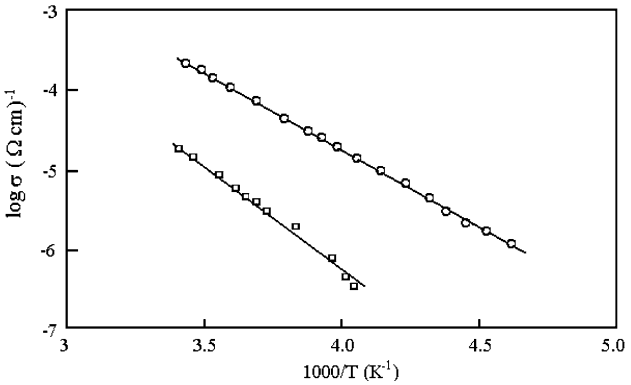

Fig. 6 Logarithm variation of the electrical conductivity versus reciprocal temperature for $Cu_{1+x}Mn_{1-x}O_2$ ($x = 0$ and 0.05)

between $Cu^{+/2+}$ in direct interaction. The combination of the ionic polarization of the surrounding oxygen octahedral around the excess charge will lead to small polaronic units.

The thermopower α of $Cu_{1.05}Mn_{095}O_2$ is positive and increases monotonically from 240 to 410 $\mu V\ K^{-1}$ (Fig. 4) indicating that the conduction should be dominated by holes with a mobility thermally activated. In such a case α is given by [23]:

$$\alpha = \frac{\Delta E_\alpha}{eT} = \frac{k}{e}\ln\frac{N_0}{N_a}$$

The density of available sites N_0 is assimilated to Cu^+ concentration ($=2.1 \times 10^{22}$ cm^{-3}) and calculated from the experimental density (5.305 cm^{-3}), N_a is the concentration of polarons (Cu^{2+}) taking part in the conduction process. Cu^{2+} ions are formed by a charge compensation mechanism when oxygen is intercalated into the host lattice or by the substitution of Mn^{3+} by Cu^{2+} and both cases would illustrate p-type conductivity. For $CuMnO_2$, N_a, deduced from the above relation, is equal 3.6×10^{19} cm^{-3} and its maximal value (6.3×10^{20} cm^{-3}) was obtained from the δ-value on the basis that each oxygen yields two holes. However, the weak ratio N_a/N_0 (0.17%) indicates that a low percentage of total number of carriers is delocalized and most of polarons are bonded (trapping of surface holes in surface-polaron states), the other values are gathered in Table 2. The structural disorder of $Cu_{1.05}Mn_{0.95}O_2$, evidenced from the absence of superstructure lines in the XRD pattern, leads to a low free path and an electron phonon mass enhancement. Taking into account the rate substitution, the average separation between foreign atoms (Cu^{2+}, Ca^{2+} or Sn^{4+}) works out to be ~1 nm assuming a random distribution. Hence, the spin polaron behaves like a heavy particle with a finite mean free path as it could be anticipated from low resistivities.

The oxygen insertion that yields further holes exert in the same time a random potential which should lead to a variable range hopping at low temperatures. Taking into

Table 2 Some physical parameters of $CuMnO_2$ based oxides

Compound	$\sigma_{300\ K}$ $(\Omega\ cm)^{-1}$	$\alpha_{300\ K}$ (μV/K)	ΔE_α (eV)	Mobility μ [cm^2 $(V\ sec)^{-1}$]	N_a/N_0 (%)
p-$CuMnO_2$	2×10^{-5}	550	0,16	3.5×10^{-6}	0.170
p-$Cu_{1.05}Mn_{0.95}O_2$	$1{,}49 \times 10^{-4}$	430	0,13	6.4×10^{-6}	0.683
p-$CuMn_{0.97}Ca_{0.03}O_2$	10^{-5}	450	0,13	5.4×10^{-7}	0.542
n-$CuMn_{0.97}Sn_{0.03}O_2$	2×10^{-6}	–750	0,22	3.53×10^{-8}	0.017

account the spin degeneracy, Doumerc [24] and later Marsh and Parish [25] have modified the Heikes formula. They have proposed an electron hopping between mixed valent states $M^{n+/(n+1)}$. For carriers moving in a narrow band (of the order of kT), S is given by

$$\alpha = (-k/e)\ln \beta(1-c)/c$$

where $\beta = (2S_e + 1)/(2S_h + 1)$ with $S_e = 1/2$ and $S_h = 0$. In the case of non-interacting electrons some carriers should be excited into CB with increasing the temperature, so c drops and α increases. c is the ratio of the number of carriers to available sites. By contrast, for $CuMnO_2$, the conductivity is thermally activated while α is nearly constant, a mechanism typical of a small polaron hopping involving a carrier concentration temperature independent. A small polaron has a high carrier concentration and a low mobility; it is formed when an electron is trapped by a local distortion; both the electron and the distortion move as a whole entity for temperatures exceeding 0.5 Θ_D, Θ_D being the Debye temperature.

The $J(V)$ plot of $CuMnO_2$ exhibits a good electrochemical stability over the whole potential range, the large current observed below –1.5 V is ascribed to H_2 evolution (H_2 bubbles were noticeable on the electrode). Under illumination, the $J(V)$ characteristic confirms clearly the p-type conductivity, i.e. the photocurrent J_{ph} starts to flow at +0.13 V and rose slowly in the negative-going potential. The localized energy levels of divalent copper ions, leading to low mobility of carriers, are responsible of the weak photocurrent. The potential (V_{on}) corresponding to photocurrent-onset J_{ph} can be reasonably employed instead V_{fb}. The difference (V_{fb} - V_{on}) generally decreased under strong light intensities. At sufficiently negative potentials J_{ph} reaches a limiting value, the magnitude of which was found to depend only on the light flux. Such behavior is ascribed to a zero recombination process of electron–hole pairs in grains boundaries. In the electrochemical scale (vs. SCE), V_{fb} outlines the position P of VB with respect to vacuum [26]:

$$P = 4.75 + eV_{fb} + \Delta E_\rho + 0.056(\mathrm{pH} - \mathrm{pzzp})$$

pzzp was estimated at 7.45 and ΔE_ρ evaluated from the linear plot $\log(1/\rho)$ vs T^{-1}. The calculated value (5.13 ± 0.15 eV) is typical of oxides in which VB is made up of 3d orbitals in contrast to O^{2-}:2p lying at ~7.2 eV below vacuum. The carriers move in a narrow bands of cationic parentage and would limit the kinetic of the global PEC process because of their low mobility, a result confirmed by the constancy of J_{ph} with the rotational frequency at a rotating electrode. Furthermore, the small decrease of dark current J_d on irradiation shutdown is an indicator of the slow transfer of excess holes. For n-$CuMn_{0.97}Sn_{0.03}O_2$, J_d is large over the whole potential range indicating that a corrosion process took place. The solution turned to brown probably because of insoluble $MnO(OH)_2$ [27], this situation looks similar to that observed over isotypic Sn-doped $CuFeO_2$ [28].

Cu^+ is d^{10} ion with a filled VB and an empty CB and the Fermi level falls in the forbidden band E_g. So, $CuMnO_2$ is expected to be semi conductor. The width of electronic bands is governed by the Cu–Cu and Cu–O bonds, determined from the degree of overlap, through which the ion B^{3+} plays an indirect role by antagonist effect. In a linear coordination field, the 3d orbital splits into a non-bonding t_{2g} level of ~2 eV above O^{2-} 2p orbital level separated by an empty hybridized Cu $4s/3d_{z^2}$ orbital forming the conduction band (CB), some 5 eV above O^{2-}:2p orbital. The advantage with the crednerite is that both VB and CB are made from orbital Cu 3d and consequently pH insensitive. Moreover, the d-character implies that the dark corrosion process is less pronounced with such oxides. On the contrary, in the absence of appropriate hole scavenger the photodissolution of $CuMnO_2$ may involve a hole transfer

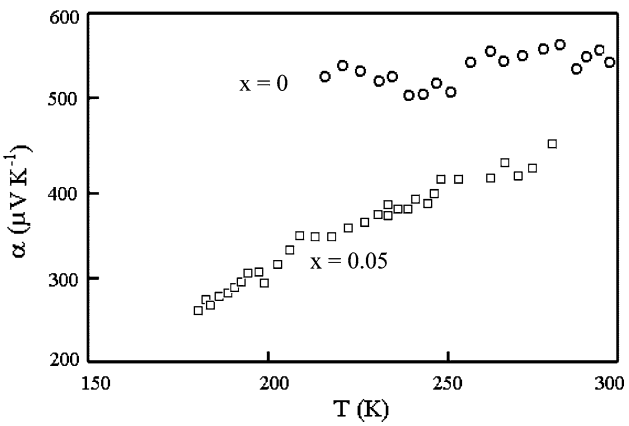

Fig. 7 The thermal variation of thermopower for $Cu_{1+x}Mn_{1-x}O_2$ (x = 0 and 0.05)

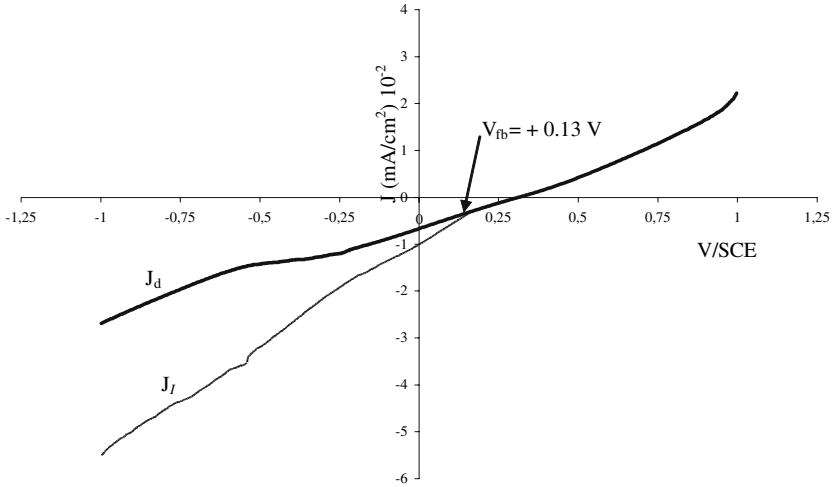

Fig. 8 Typical $J(V)$ curve of $Cu_{1.05}Mn_{0.95}O_2$ in the dark and under illumination, scan rate 5 mV s^{-1}

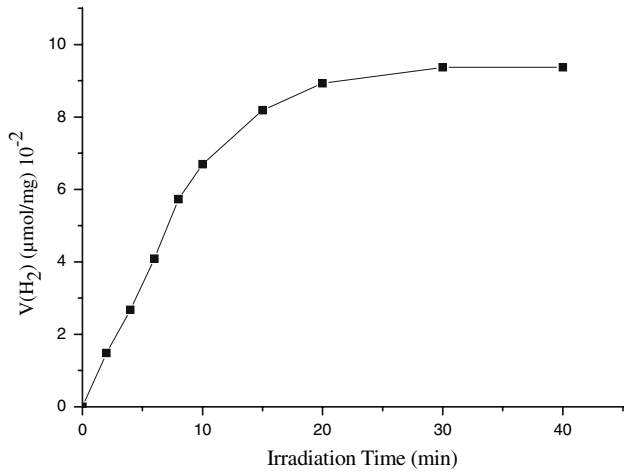

Fig. 9 H_2 evolution from aqueous suspension of $CuMnO_2$ in S^{2-} media (pH 13.62)

pathway. The powder immersed in KCl solution turned to blue when exposed to visible light ($Cu^{+}_{lattice} \rightarrow Cu^{2+}_{solution}$).

An instructive comparison could be made with the nearest $CuCrO_2$. As Mn–O is more covalent than Cr–O (chromium is more electronegative). The splitting between non-bonding t_{2g} VB, constant in energy regardless of the nature of B metal, and σ^* forming CB and arising from a mixing $4s/3d_{z^2}$ orbitals increases, this results in a destabilization of CB with a larger E_g value (1.28 eV) [13] compared to $CuMnO_2$ (1 eV $\approx 2\Delta E_\rho$). The IR spectra seem to corroborate this conclusion; the isomer shift toward lower wave numbers of $CuCrO_2$ (625.6 cm^{-1}) compared to $CuMnO_2$ (659.5 cm^{-1}) means that the length Cu–O is smaller (0.1834 nm) in $CuMnO_2$ with respect to $CuCrO_2$ (0.1854 nm) and this would have the effect to raise CB of d/s parentage leading normally to a larger gap E_g.

Hydrogen formation over cheap raw oxides remains an attractive and challenging project. As application, $CuMnO_2$ was used for the visible light induced water reduction with concomitant oxidation of S^{2-}, an issue of environmental field. The separation of electron–hole pairs occurs exclusively in the depletion layer W through the internal junction field whereas the most part is lost outside the diffusion length L_D by recombination. The low carrier mobility makes the length L_D small and for low polarons hopping SC, it was interesting to prepare the oxide by exchange reaction. This allows a minimization of both the electric resistance and the carriers paths. The crystallite size must be comparable with the width W and does not block the photocurrent. $CuMnO_2$ is long lived, absorbs a large part of the sun spectrum and is promising for bias free solar cathode. Moreover, the electron affinity can be raised by using cations of small ionization energy, an advantageous feature for p-type specimen. It seemed attractive to take advantage of the pH-insensivity of electronic bands to move up the potential of H_2O/H_2 couple above CB by working in basic media and where the water reduction would proceed with low over voltages. For $CuMnO_2$, the free potential U_f (–0.375 V) is negative of V_{fb} and should give rise to a large band bending in presence of a high negative potential such as S_n^{2-}/S^{2-} (~–0.77 V). The key finding is that S^{2-} ions enable $CuMnO_2$ to be photo electrochemically stable and make the potential V_{fb} shift towards the anodic direction. Figure 7 shows the volume of evolved vs. time illumination in powder suspension; a quantum efficiency 0.575% was found under polychromatic light (Figs. 8 and 9).

Conclusion

We successfully synthesized the crednerite $CuMnO_2$ by $Cu^{+} \rightarrow Li^{+}$ exchange reaction. The monoclinic distortion results from a strong Y–T-like elongation of MnO_6 octahedra. The magnetic data are consistent with the ionic configuration $Cu^{I}Mn^{III}O_2$ and HS moment of Mn^{3+}. The susceptibility showed a typical feature of low dimensionality

with strong intraplane antiferromagnetic interactions where the exchange occurred between half filled d_{z^2} orbitals. $CuMnO_2$ is a candidate for a two-dimensional antiferromagnetic lattice. The electrical properties vary slightly by doping with non-isovalent ions and/or by oxygen insertion. As prepared, it exhibits a *p*-type conductivity confirmed by a positive thermopower and a cathodic direction of photocurrent. The large ΔE-values are in conformity with a conduction mechanism by low polarons hopping involving only nearest neighbors. The linear increase of thermopower for doped oxide with the temperature indicates a mobility thermally activated. The low electron mobility is due to the obstruction of oxygen octahedra to hopping process between manganese ions. The weak covalent character of Mn-O bond resulted in a destabilization of σ^* CB and a decrease of optical gap compared to $CuCrO_2$. $CuMnO_2$ has a structure containing linear CuO_2^{3-} units, which determine that both the valence and conduction bands are of Cu 3d parentage and pH-independent through which the CB edge can be properly matched to H_2O/H_2 level. The photo electrochemical process is controlled kinetically by the electrons supply at the interface. Photoactive $CuMnO_2$ is low cost, absorb a large part of the solar spectrum and is a potential material for bias free photocathode. It was tested positively for the hydrogen generation upon visible light.

Acknowledgements This work was financially supported by the Faculty of Chemistry (Algiers) under the contact No. E1602/07/04. The authors would like to thank B. Biri for his technical assistance and helpful discussions.

References

1. Turner JA (2004) Science 305:972
2. Marquardt MA, Ashmore NA, Cann DP (2006) Thin Solid Films 496:146
3. Li J, Sleight AW, Jones CY, Toby BH (2005) J Solid State Chem 178:285
4. Doumerc JP, Wichainchai A, Ammar A, Pouchard M, Hagenmeller P (1986) Mater Res Bull 21:745
5. Subrahmanyam A, Barik UK (2005) J Phys Chem Solids 66:817
6. Bruce Gall R, Nathan Ashmore, Meagen Marquardt A, Xiaoli Tan, David P (2005) Can J Alloys Compd 391:262
7. Younsi M, Aider A, Bouguelia A, Trari M (2005) Solar Energy 78:574
8. Bessekhouad Y, Trari M, Doumerc JP (2003) Int J Hydrogen Energy 28:43
9. Shin YJ, Doumerc JP, Dordor P, Delmas C, Pouchard M, Hagenmuller P (1993) J Solid State Chem 107:303
10. Doumerc JP, Trari M, Töpfer J, Fournès L, Grenier JC, Pouchard M, Hagenmuller P (1994) Eur J Solid State Chem 31:705
11. Stanley KJ (1972) Oxide magnetic materials. Clarendon, Oxford
12. Dordor P, Marquestaut E, Villeneuve G (1980) Rev Phys Appl 15:1607
13. Saadi S, Bouguelia A, Trari M (2006) Solar Energy 80:272
14. Trari M, Töpfer J, Dordor P, Grenier JC, Pouchard M, Doumerc JP (2005) J Solid State Chem 178:2751
15. Töpfer J, Trari M, Gravereau P, Chaminade JP, Doumerc JP (1995) Z Krist 210:184
16. Shannon RD (1976) Acta Cryst A 32:751
17. Koriche N, Bouguelia A, Trari M (2007) J Mater Sci, doi:10.1007/s10853-006-0741-0
18. Nyquist RA, Kagel RO (1971) Infrared spectra of inorganic compounds. Academic Press, New York
19. Trari M (1994) Ph.D Thesis, Bordeaux University
20. Kittel C (1988) Physique de l'Etat Solide, Dunod Université
21. Lide DR (Editor in Chief) (1997–1998) Handbook of chemistry and physics, 78th edn. CRS press
22. Rogers DB, Shannon RD, Prewitt CT, Gillson JL (1971) Inorg Chem 10:723
23. Trestmann-Matts V, Dorris SE, Kumarakrishnan S, Mason TO (1983) Am J Ceram Soc 66:829
24. Doumerc JP (1994) J Solid State Chem 110:419
25. Marsh DB, Parris PE (1996) Phys Rev B 54(11):7720
26. Butler MA, Ginley DS (1980) J Electrochem Soc 127:1273
27. Alexéev V (1976) Analyse qualitative, ed. Mir
28. Benko FA, Koffyberg FP (1987) J Phys Chem Solids 48:431